

# Lawrence Berkeley National Laboratory

LBL Publications

## Title

Investigating the Urban Air Quality Effects of Cool Walls and Cool Roofs in Southern California

## Permalink

<https://escholarship.org/uc/item/0s45z1hk>

## Journal

Environmental Science and Technology, 53(13)

## ISSN

0013-936X

## Authors

Zhang, Jiachen

Li, Yun

Tao, Wei

et al.

## Publication Date

2019-07-02

## DOI

10.1021/acs.est.9b00626

Peer reviewed

This document is a pre-print of the following publication:

Zhang, J., Li, Y., Tao, W., Liu, J., Levinson, R., Mohegh, A., & Ban-Weiss, G. (2019). Investigating the Urban Air Quality Effects of Cool Walls and Cool Roofs in Southern California. *Environmental Science & Technology*, 53(13), 7532–7542.  
<https://doi.org/10.1021/acs.est.9b00626>

The pre-print may lack improvements made during the typesetting process. If you do not have access to the publication, you may request it from Ronnen Levinson at Lawrence Berkeley National Laboratory ([RML27@cornell.edu](mailto:RML27@cornell.edu)).

1 **Investigating the urban air quality effects of cool walls and cool roofs in**  
2 **Southern California**

3 Jiachen Zhang<sup>1</sup>, Yun Li<sup>1</sup>, Wei Tao<sup>2</sup>, Junfeng Liu<sup>3</sup>, Ronnen Levinson<sup>4</sup>, Arash Mohegh<sup>1</sup>, George Ban-  
4 Weiss<sup>1,\*</sup>

5 <sup>1</sup> Department of Civil and Environmental Engineering, University of Southern California, Los Angeles,  
6 CA, USA

7 <sup>2</sup> Multiphase Chemistry Department, Max-Planck-Institute for Chemistry, Hahn-Meitner-Weg 1, Mainz,  
8 Germany

9 <sup>3</sup> Laboratory for Earth Surface Processes, College of Urban and Environmental Sciences, Peking  
10 University, Beijing, China

11 <sup>4</sup> Heat Island Group, Lawrence Berkeley National Laboratory, Berkeley, CA, USA

12 \*Correspondence to George Ban-Weiss, banweiss@usc.edu, 213-740-9124

13

14 **Abstract**

15 Solar reflective cool roofs and walls can be used to mitigate the urban heat island effect. While  
16 many past studies have investigated the climate impacts of adopting cool surfaces, few studies  
17 have investigated their effects on air pollution, especially on particulate matter (PM). This  
18 research for the first time investigates the influence of widespread deployment of cool walls on  
19 urban air pollutant concentrations, and systematically compares cool wall to cool roof effects.  
20 Simulations using a coupled meteorology-chemistry model (WRF-Chem) for a representative  
21 summertime period show that cool walls and roofs can reduce urban air temperatures, wind

22 speeds, and planetary boundary heights in the Los Angeles Basin. Consequently, increasing wall  
23 (roof) albedo by 0.80, an upper bound scenario, leads to maximum daily 8-hour average ozone  
24 concentration reductions of 0.35 (0.83) ppbv in Los Angeles County. However, cool walls  
25 (roofs) increase daily average PM<sub>2.5</sub> concentrations by 0.62 (0.85)  $\mu\text{g m}^{-3}$ . We investigate the  
26 competing processes driving changes in concentrations of speciated PM<sub>2.5</sub>. Increases in primary  
27 PM (elemental carbon and primary organic aerosols) concentrations can be attributed to  
28 reductions in ventilation of the Los Angeles Basin. Increases in concentrations of semi-volatile  
29 species (e.g., nitrate) are mainly driven by increases in gas-to-particle conversion due to reduced  
30 atmospheric temperatures.

31

## 32 1 Introduction

33 Urbanization is occurring at a fast pace around the world; global urban land area in 2030 is  
34 projected to be up to triple that in 2000<sup>1</sup>. Compared to rural areas with natural land cover, urban  
35 areas contain more impervious surfaces that are made of solar absorptive and thermally massive  
36 materials, such as asphalt concrete. Urban areas also contain less vegetation and thus reduced  
37 evaporative cooling and shade cover. These differences in urban and natural land cover contribute  
38 to the urban heat island (UHI) effect (i.e., cities being hotter than their surrounding rural areas)<sup>2</sup>,  
39 which can, in turn, affect air pollutant concentrations. The air quality effects of urban land  
40 expansion have been studied in previous research<sup>3-7</sup>, although only a few studies clearly explained  
41 the mechanisms driving these effects<sup>8-11</sup>. Tao et al.<sup>8</sup> suggested that with pollutant emissions held  
42 constant, urbanization in eastern China would increase ozone concentrations from the surface to 4

43 km. However, it would also enhance turbulent mixing and vertical advection, therefore reducing  
44 the concentrations of primary pollutants below 500 m.

45 While many studies have explored the air quality impacts of the UHI effect, fewer studies have  
46 investigated how strategies that mitigate the UHI effect would influence urban air quality<sup>12-15</sup>. For  
47 example, adopting solar reflective cool surfaces (roofs, walls, and pavements) increases city albedo  
48 and the solar radiation reflected by cities, therefore reducing urban surface temperatures and near-  
49 surface air temperatures<sup>16-22</sup>. However, adopting cool surfaces might change air quality in  
50 unexpected ways. For primary pollutants (i.e., pollutants directly emitted to the atmosphere) such  
51 as elemental carbon (EC), nitric oxide (NO), and carbon monoxide (CO), lower surface  
52 temperatures in cities may suppress convection and therefore reduce atmospheric mixing heights  
53 and vertical dispersion of pollutants, leading to increases in pollutant concentrations near the  
54 ground<sup>23</sup>. Changes in horizontal temperature distributions can also influence wind speed and  
55 direction, affecting the horizontal transport and distribution of pollutants. For secondary pollutants  
56 (i.e., pollutants formed in the atmosphere from primary pollutants), in addition to the previously  
57 mentioned changes in transport and dispersion of pollutants and their precursors, pollutant  
58 concentrations can also be influenced by temperature dependent chemical reactions, phase-  
59 partitioning, and emissions. Tropospheric ozone is primarily formed via reactions between  
60 nitrogen oxides (NO<sub>x</sub>) and volatile organic compounds (VOCs). Reductions in dispersion could  
61 increase both VOC and NO<sub>x</sub> concentrations, though impacts on ozone could be counterintuitive  
62 due to non-linearities in ozone chemistry. Lowering air temperature decreases biogenic VOC  
63 emissions from vegetation, potentially reducing ozone concentrations in urban areas where VOC  
64 availability limits ozone formation<sup>24</sup>. Air temperature reduction also slows reactions that produce  
65 ozone. Therefore, ozone concentrations are expected to decrease with lower temperatures<sup>25</sup>.

66 Secondary particulate matter includes sulfate, nitrate, ammonium, and secondary organic aerosols  
67 (SOA). While temperature-dependent reactions that form secondary particulate matter should be  
68 slower due to reduced temperatures, gas-particle partitioning for semi-volatile species (ammonium  
69 nitrate and semi-volatile SOA) favors the particle phase<sup>26,27</sup>. The competing physical and chemical  
70 processes lead to uncertainties in changes to air pollution concentrations induced by heat island  
71 mitigation strategies.

72 The complexity of the aforementioned processes requires the use of sophisticated models that  
73 resolve atmospheric physics and chemistry to predict how cool surface adoption would influence  
74 city-level air quality. Using photochemical models, Taha et al.<sup>13,28</sup> estimated that increasing city  
75 surface albedo would effectively reduce ozone concentrations in Southern California and Central  
76 California. Epstein et al.<sup>23</sup> predicted that 8-hour daily maximum ozone concentrations would  
77 decrease if cool roofs do not reflect more solar ultraviolet (UV) than do dark roofs; if solar UV  
78 reflection is increased, ozone concentrations could rise.

79 Despite previous literature on the influence of cool roofs on ozone concentrations, there is only  
80 one study that has investigated the influence of cool roofs on particulate matter<sup>23</sup>. They found that  
81 increasing roof albedo would increase the annual mean concentrations of PM<sub>2.5</sub>, because reduced  
82 ventilation would suppress dispersion of pollutants. However, they did not investigate (1) the  
83 various physicochemical processes driving cool roof impacts on PM<sub>2.5</sub> concentrations or (2) the  
84 varying responses of different PM species (e.g., nitrate, sulfate, and organics) to cool roof adoption.

85 Cool walls are less studied than cool roofs. Zhang et al.<sup>29</sup>, for the first time, estimated the influence  
86 of cool walls on urban climate, and systematically compared the effects of cool walls to cool roofs.  
87 They found that adopting cool walls in Los Angeles would lead to daily average canyon air

88 temperature reductions of up to 0.40 K, which is slightly lower than that induced by adopting cool  
89 roofs (0.43 K). However, the influence of cool walls on air quality has never been studied.

90 To address the aforementioned science knowledge gaps and inform policymaking on heat  
91 mitigation strategies, we seek to (1) quantify and systematically compare the air quality effects of  
92 adopting cool walls and roofs, and (2) investigate the physicochemical processes leading to  
93 changes in particulate matter concentrations.

94

## 95 2 Method

### 96 2.1 Model description

97 We use the Weather Research and Forecasting model coupled with Chemistry Version 3.7 (WRF-  
98 Chem V3.7), a state-of-the-science climate and air quality model, to estimate the impacts of  
99 employing cool walls and roofs on air quality<sup>30</sup>. WRF-Chem has been widely used to study air  
100 pollution in Southern California<sup>11,31,32</sup>. Table S2 summarizes our model configuration. The  
101 following schemes are chosen for WRF physics: the Rapid Radiative Transfer Model (RRTM) for  
102 long-wave radiation<sup>33</sup>, the Goddard shortwave radiation scheme<sup>34</sup>, the Lin et al. scheme<sup>35</sup> for cloud  
103 microphysics, the Grell 3D ensemble cumulus cloud scheme<sup>36</sup>, and the Yonsei University scheme  
104 for the planetary boundary layer<sup>37</sup>.

105 Impervious fraction (Figure S3b) and land use classification in urban grid cells (Figure S3c) are  
106 obtained from the National Land Cover Database (NLCD, 2006)<sup>38,39</sup>. The Noah land surface  
107 model<sup>40</sup> simulates land-atmosphere interactions in non-urban grid cells and for the pervious  
108 portion of urban grid cells. The single-layer urban canopy model resolves urban physics and

109 simulates land-atmosphere interactions for the impervious portion of urban grid cells<sup>41</sup>. Urban grid  
110 cells are classified as low-intensity residential (“Developed, Open Spaces” and “Developed, Low  
111 Intensity” in NLCD), high-intensity residential (“Developed, Medium Intensity” in NLCD), and  
112 commercial/industrial (“Developed, High Intensity” in NLCD). Urban morphology (i.e., roof  
113 width, canyon floor width, and building height) is determined for each urban land use type based  
114 on real-world building and street datasets for Los Angeles County, following Zhang et al<sup>29</sup>; the  
115 datasets include National Urban Database and Access Portal (NUDAPT)<sup>42</sup>, the Los Angeles  
116 Region Imagery Acquisition Consortium (LARIAC)<sup>42</sup>, and LA County Street and Address File<sup>43</sup>.  
117 Since the default WRF-Chem is not compatible with the NLCD land use classification system, we  
118 modify the model code to allow for use of NLCD urban land use types, following Fallmann et  
119 al.<sup>44</sup>. We also implement satellite-based green vegetation fraction into the model following  
120 Vahmani and Ban-Weiss<sup>21</sup>.

121 Gas phase chemistry is simulated using the Regional Atmospheric Chemistry Mechanism  
122 (RACM)<sup>45</sup> scheme, further updated by National Oceanic and Atmospheric Administration  
123 (NOAA) Earth System Research Laboratory (ESRL)<sup>32</sup>. The RACM-ESRL scheme covers organic  
124 and inorganic chemistry simulating 23 photolysis and 221 other chemical reactions<sup>46</sup>. The Modal  
125 Aerosol Dynamics Model for Europe (MADE) simulates aerosol chemistry<sup>47</sup>. The volatility basis  
126 set (VBS) is used for simulating secondary organic aerosols<sup>48</sup>.

127 We evaluate modeled ozone and PM<sub>2.5</sub> concentrations against observations (Figures S1 and S2,  
128 Table S1) from the Environmental Protection Agency’s Air Quality System in Section S1 of the  
129 Supporting Information. Although our model underestimates ozone and PM<sub>2.5</sub> concentrations at  
130 higher concentrations, the bias in baseline concentrations does not necessarily lead to bias in  
131 estimated changes induced by adopting cool surfaces.



132

## 133 2.2 Simulation domains

134 We simulate three nested domains (d1, d2, and d3, as shown in Figure S3a) with 30 layers in the  
135 vertical at horizontal resolutions of 18 km, 6 km, and 2 km, respectively. The three domains each  
136 cover the Southwestern United States (d1); Central and Southern California (d2); and Southern  
137 California, including Los Angeles and San Diego (d3). Each outer domain provides boundary  
138 conditions for the adjacent inner domain. In this paper we report results for the innermost domain.

139

## 140 2.3 Emission inventories

141 WRF-Chem requires gridded emissions inputs for each simulation. We use state-of-the-science  
142 emission inventories from the South Coast Air Quality Management District (SCAQMD) and  
143 California Air Resources Board (CARB) for the year 2012 (i.e., the most up-to-date inventories as  
144 of writing this paper). For the outer two domains (d1 and d2), hourly emissions for the entire year  
145 at 4-km resolution are provided by CARB for California<sup>49</sup>. Emissions outside California, but  
146 within the simulation domain, are from National Emissions Inventory (NEI) by the Environmental  
147 Protection Agency for the year 2011<sup>50</sup>. For the innermost domain (d3), we use hourly emissions  
148 for the entire year at 4-km resolution provided by SCAQMD<sup>51</sup>. These emissions represent all  
149 anthropogenic sources including motor vehicles; point sources such as refineries; and off-road  
150 sources, such as construction. Emission inventories are regridded to match the grid for the modeled  
151 domains and chemical speciation for RACM-ESRL and MADE/VBS mechanisms used in this  
152 study. The Model of Emissions of Gases and Aerosols from Nature (MEGAN) is used to generate  
153 temperature-dependent biogenic organic emissions<sup>52</sup>. Note that anthropogenic emissions are not

154 sensitive to ambient temperatures in our study. Though some anthropogenic emissions may be  
155 temperature dependent (e.g., evaporative emissions of VOCs from gasoline powered vehicles),  
156 this effect is not simulated in this study, as anthropogenic emissions are obtained directly from  
157 input datasets.

158

## 159 2.4 Simulation design

160 To investigate the air quality effects of cool walls and roofs in Southern California, we simulate  
161 three scenarios: CONTROL, where wall, roof, and pavement albedos are each set to 0.10;  
162 COOL\_WALL, where wall albedo is increased to 0.90; and COOL\_ROOF, where roof albedo is  
163 increased to 0.90. These cool surface albedos are intentionally chosen to quantify the upper bound  
164 effects of adopting cool surfaces (i.e., increasing surface albedo by 0.80). Note that cool surface  
165 albedos of actual cool walls and roofs are usually lower than 0.90. For example, the albedo of a  
166 bright-white cool roof may decrease to 0.60–0.70 from an initial albedo of 0.80–0.90 after several  
167 years of soiling and weathering<sup>53,54</sup>. In order to test the linearity of changes in air pollutant  
168 concentrations to albedo increases, we add two additional scenarios where wall albedo and roof  
169 albedo are each increased by 0.40.

170 Simulations are performed for 28 June 2012 to 11 July 2012, with the first five days discarded as  
171 model “spin-up” to reduce the possible influence of inaccuracies in input initial conditions on our  
172 analysis. We analyze the results from 00:00 local standard time (LST) on July 3 to 00:00 LST on  
173 July 12. Section S3 in the Supporting Information demonstrates that the meteorology during our  
174 analysis period is representative of summertime meteorology in Southern California. Thus, our  
175 results are representative of changes induced by adopting cool surfaces under typical summertime

176 conditions in Southern California. The paired Student's t-test ( $n = 9$  analyzed days) is used to  
177 assess whether the changes in cool surface scenarios relative to CONTROL are statistically  
178 distinguishable from zero.

179

## 180 2.5 Method of attributing the changes in PM to ventilation versus other 181 factors

182 Carbon monoxide (CO) is considered a chemically inert pollutant at urban scale, with  
183 concentrations controlled by meteorological conditions. Therefore, past studies have used CO as  
184 a tracer for transport and dispersion of pollutants<sup>9,56</sup>. Similarly, in our study, we use the increase  
185 in CO concentration relative to CONTROL to quantify the increase in PM<sub>2.5</sub> that is attributable to  
186 ventilation ( $\Delta C_{PM(\text{vent})}$ ), as

$$\Delta C_{PM(\text{vent})} = \frac{\Delta C_{CO}}{C_{CO}} \times C_{PM} \quad (1)$$

187 where  $\Delta C_{CO}$  is the change in CO mixing ratio (ppbv) relative to CONTROL,  $C_{CO}$  is the mixing  
188 ratio (ppbv) of CO for CONTROL,  $C_{PM}$  is the concentration ( $\mu\text{g m}^{-3}$ ) of a PM species (i.e., total  
189 PM<sub>2.5</sub>, sulfate, nitrate, elemental carbon, primary organic aerosol, anthropogenic secondary  
190 organic aerosols, or biogenic secondary organic aerosols) for CONTROL, and all variables are  
191 spatial averages over urban areas in Los Angeles County.

192 The change in concentration of a PM<sub>2.5</sub> species that is not attributable to ventilation  $\Delta C_{PM(\text{no vent})}$   
193 ( $\mu\text{g m}^{-3}$ ) is then calculated as

$$\Delta C_{PM(\text{no vent})} = \Delta C_{PM} - \frac{\Delta C_{CO}}{C_{CO}} \times C_{PM} \quad (2)$$

194

195 In this way, we attribute increases in PM<sub>2.5</sub> species to reductions in ventilation and changes in all  
196 other processes. Note that while sea salt aerosols contribute to total PM<sub>2.5</sub> concentrations, we omit  
197 this species from the discussion because they are naturally produced and are not a public health  
198 concern. Reductions in ventilation may also contribute to less vertical mixing and consequent  
199 reductions in dry deposition of pollutants.

## 200 2.6 Caveats

201 In this study, we assume that adopting cool surfaces would not change reflectance in the UV  
202 spectrum (280–400 nm). However, based on spectral reflectance measurements, UV reflectance  
203 could increase from adopting cool roofs<sup>23</sup>. Increases in UV reflectance could enhance ozone  
204 production and atmospheric oxidation capacity, which influences the formation of other secondary  
205 pollutants. Therefore, changes in ozone are a result of competing effects among (a) ozone increases  
206 induced by enhanced UV reflection, (b) ozone decreases induced by decreased temperatures, and  
207 (c) ozone changes induced by reduced ventilation, which could affect the dispersion of ozone and  
208 its precursors.

209 The influence of adopting cool surfaces is likely to vary by city due to differences in baseline  
210 climate and land cover (e.g., vegetation distributions, building distributions, urban canyon  
211 morphology). Also note that results might be different if simulated using another model or using  
212 different parameterizations. For example, the single layer urban canopy model does not explicitly  
213 resolve individual buildings.

214 Note that the urban morphology is derived using gross wall area (including windows) instead of  
215 net wall area (excluding windows). In Los Angeles County, citywide ratio of net wall area to gross  
216 wall area is 83%.<sup>29</sup> In reality, windows may not be changed to cool colors. Therefore, a portion of

217 walls may not be able to be made solar reflective and our study may overestimate the influence of  
218 adopting cool walls.

219

## 220 3 Results and discussion

221 By comparing changes in air pollutant concentrations for increasing albedo by 0.80 versus 0.40  
222 relative to CONTROL, we find that the changes in air pollutant concentrations are approximately  
223 linear to surface albedo change (Section S4 in the Supporting Information). Therefore, the results  
224 reported for albedo increase of 0.80 can be interpolated to other albedo changes. For simplicity,  
225 we report only results for COOL\_WALL and COOL\_ROOF in the main body.

### 226 3.1 Meteorological conditions

227 Figure 1 shows spatial distributions of near-surface air temperatures in the afternoon and evening.  
228 (Diurnal cycles of near-surface air temperatures are shown in Figure S4.) For the CONTROL  
229 scenario (Figure 1a), temperatures in inland areas are hotter than coastal areas, as expected.  
230 Temperature reductions induced by adopting cool surfaces are higher in inland areas than in coastal  
231 areas (Figure 1b,c). This is due to an accumulation effect in air temperature reduction as the sea  
232 breeze advects air from the coast to inland.

233 Although total wall area in Los Angeles County is larger than roof area by a factor of 1.7, daily  
234 average solar irradiance ( $\text{W m}^{-2}$ ) on walls is 38% of that on roofs<sup>29</sup>. In addition, 50-59% of the  
235 solar radiation reflected by cool walls is absorbed by opposing walls or pavements, while all the  
236 radiation reflected by cool roofs escapes the urban canopy in the model<sup>29</sup>. Therefore, daily average  
237 temperature reductions induced by cool roofs (0.45 K) are larger than cool walls (0.24 K) over

238 urban areas in Los Angeles County, as shown in Table 1. Cool roofs are simulated to induce larger  
239 temperature reductions than cool walls at both 14:00 LST (daytime) and 20:00 LST (nighttime).

240 Note that past studies investigating how air temperatures influence atmospheric chemistry often  
241 report 2-meter air temperatures (“T2”)<sup>8,45</sup>. However, 2-meter air temperature is a diagnostic  
242 variable that is not used in model calculations of atmospheric chemistry. The chemistry model  
243 actually uses the four-dimensional (x, y, z, t) atmospheric temperature. Therefore, we present  
244 temperatures in the lowest atmospheric layer as “near-surface air temperature” rather than “T2.”

245 Figures S5 and S6 show diurnal cycles and spatial maps of 10-meter horizontal wind speeds, and  
246 Figure S7 shows horizontal wind vectors. For the CONTROL scenario, winds are southwesterly  
247 from coast to inland and wind speed is higher during daytime than nighttime. As shown in Table  
248 1, spatially averaged wind speed in urban areas is 4.2 m s<sup>-1</sup> and 2.3 m s<sup>-1</sup> at 14:00 LST and 20:00  
249 LST, respectively. Simulations predict that adopting cool walls (roofs) decreases onshore wind  
250 speeds by 0.06 (0.21) m s<sup>-1</sup> at 14:00 LST and 0.08 (0.09) m s<sup>-1</sup> at 20:00 LST. This can be explained  
251 by the reduced temperature difference between urban land and ocean, which is a driver for the sea  
252 breeze.

253 Figure S8 show the diurnal cycle of planetary boundary layer (PBL) height. PBL height reaches  
254 its maximum at 12:00 LST. Adopting cool walls reduces PBL height by 3-7% at most times of  
255 day. Adopting cool roofs reduces PBL height by about 5% at night and about 10% during the day.  
256 The reduction in PBL height can be attributed to decreases in surface temperatures and consequent  
257 reductions in convection. Decreases in wind speeds and PBL height tend to reduce ventilation for  
258 pollutants. The influence of changes in ventilation on particulate matter is discussed in Section  
259 3.5.1.

260

## 261 3.2 Spatial distribution of ozone concentrations

262 Figure 2 shows the spatial distribution of daily maximum 8-hour average (MDA8) ozone  
263 concentrations. MDA8 ozone is regulated by the National Ambient Air Quality Standards of the  
264 Environmental Protection Agency. For the CONTROL scenario, the ozone concentration over  
265 urban areas is lower than rural areas because (a) southwesterly winds transport ozone and its  
266 precursors from the coast to the inland areas, creating an accumulation effect as this secondary  
267 pollutant is generated in the atmosphere; and (b) nitric oxide emissions in urban areas can titrate  
268 ozone. Adopting cool walls can decrease the spatially averaged MDA8 ozone concentration by  
269 0.35 ppbv in the urban areas of Los Angeles County (Table 1). These decreases in ozone  
270 concentrations are likely due to reductions in temperature-dependent ozone formation. Adopting  
271 cool roofs can lead to a greater reduction in MDA8 ozone concentration (0.83 ppbv) than cool  
272 walls. This is likely because the near-surface air temperature reductions induced by cool roofs are  
273 larger than that induced by cool walls during daytime (Figure S4) and thus the decreases in reaction  
274 rates for ozone production are larger for COOL\_ROOF than COOL\_WALL relative to CONTROL.  
275 As mentioned in Section 2.5, we assume that the UV reflectance of cool surfaces is the same as  
276 dark surfaces. Similarly, Epstein et al<sup>23</sup> report reductions in ozone concentrations in most Southern  
277 California regions due to adopting cool roofs when UV reflectance is assumed to be held constant.  
278 (Note that they also find that ozone concentrations could increase if the difference in UV  
279 reflectance between cool and dark roofs follows an upper bound scenario.)

280

### 281 3.3 Spatial distribution of PM<sub>2.5</sub> species

282 Figure 3 shows the spatial distribution of daily average PM<sub>2.5</sub> species concentrations and changes  
283 due to adopting cool surfaces. PM<sub>2.5</sub> concentrations reported here represent dry particle mass.  
284 Spatial distributions of PM<sub>2.5</sub> species concentrations in the CONTROL scenario are mainly  
285 attributable to spatial patterns in emissions and meteorology. For example, when the sea breeze  
286 advects air from the coast to inland, EC, a primary pollutant, accumulates, leading to higher  
287 concentrations in locations further east. For spatial distributions of sulfate concentrations, there  
288 are higher concentrations near the ports of Los Angeles and Long Beach that are likely due to hot  
289 spots in SO<sub>2</sub> (the precursor of secondary sulfate) and primary sulfate emissions from ships and  
290 power plants (Figure S9). Meanwhile, southwesterly winds then transport these emissions to  
291 downtown Los Angeles, making concentrations downtown greater than those further east. The  
292 spatial variability of anthropogenic and biogenic SOA is relatively small compared to other species.

293 The concentrations of total PM<sub>2.5</sub> and each individual species increase due to cool surface adoption  
294 (Figure 3). The increase in each PM<sub>2.5</sub> species induced by adopting cool roofs is larger than that  
295 induced by cool walls, though their spatial patterns are similar. Spatial distributions of increases  
296 in total PM<sub>2.5</sub> and individual species (except nitrate) are consistent with the spatial patterns of  
297 absolute concentrations in the CONTROL scenario. In other words, the regions with the highest  
298 baseline concentrations show the largest changes in PM<sub>2.5</sub> due to meteorological shifts from cool  
299 surface adoption. The exception is for nitrate, which shows larger increases in urban residential  
300 areas northeast of downtown where baseline concentrations are low, rather than downtown where  
301 baseline concentrations are the highest in CONTROL. This is likely due to the greater temperature  
302 reductions in regions northeast of downtown Los Angeles relative to downtown, especially at night  
303 (Figure 1b,c). The processes leading to nitrate increases will be discussed in Section 3.5. The



304 increase in SOA is relatively smaller than other species, which will also be explained in Section  
305 3.5.

### 306 3.4 Diurnal cycles of PM<sub>2.5</sub> species concentrations

307 Figure 4 shows the diurnal cycles of spatially averaged PM<sub>2.5</sub> species concentrations and their  
308 changes in the urban areas of Los Angeles County. For the CONTROL scenario, PM<sub>2.5</sub>, nitrate,  
309 ammonium, sulfate, EC, and primary organic aerosol (POA) concentrations reach their maximum  
310 between 08:00 and 09:00 LST and their minimum at 16:00 LST, while biogenic and anthropogenic  
311 SOA reach their maximum near 14:00 LST and their minimum at night. The diurnal cycles of  
312 PM<sub>2.5</sub> concentrations can be attributed to the diurnal variation of (1) emissions (Figure S10); (2)  
313 PBL height (Figure S8a), which peaks at 12:00 LST; (3) wind speed (Figure S5), which peaks at  
314 14:00 LST; and (4) photochemical reaction rates for secondary species that depend on UV  
315 radiation and temperature (Figure S4a).

316 Raising roof or wall albedo leads to increases in concentrations of total PM<sub>2.5</sub> and most individual  
317 species (except for biogenic SOA) throughout the day (Figure 4). Increases in nitrate  
318 concentrations are the largest among all PM<sub>2.5</sub> species, followed by increases in POA, sulfate, and  
319 ammonium, while the increases in concentrations of other PM<sub>2.5</sub> species are relatively small. The  
320 changes in speciated PM<sub>2.5</sub> concentrations due to adopting cool walls or roofs vary by time of day,  
321 and the mechanisms contributing to the changes will be discussed in Section 3.5. For all PM<sub>2.5</sub>  
322 species except biogenic SOA, increases in PM<sub>2.5</sub> concentrations induced by adopting cool roofs  
323 are larger than those induced by adopting cool walls during most daytime hours (07:00-19:00 LST).  
324 On daily average, cool roof adoption contributes to greater increases in particulate matter than cool  
325 wall adoption (Table 1) for total PM<sub>2.5</sub> and each species. Daily average increases in total PM<sub>2.5</sub>  
326 concentrations are simulated to be 0.62 (0.85)  $\mu\text{g m}^{-3}$  upon increasing wall (roof) albedo by 0.80

327 in July in Los Angeles County. Compared to the national annual and 24-hour  $\text{PM}_{2.5}$  standard of 12  
328  $\mu\text{g m}^{-3}$  and  $35 \mu\text{g m}^{-3}$ , respectively, increases in  $\text{PM}_{2.5}$  concentrations reported here have the  
329 potential for increasing exceedance days of federal air quality standards. The grid cell containing  
330 Mira Loma (i.e., the most polluted  $\text{PM}_{2.5}$  monitoring station in Southern California) is simulated  
331 to have  $\text{PM}_{2.5}$  increases of  $0.84 (1.05) \mu\text{g m}^{-3}$  due to adopting cool walls (roofs) in summer. Epstein  
332 et al. (2018) estimate that annual average  $\text{PM}_{2.5}$  concentrations at Mira Loma would increase by  
333  $0.19 \mu\text{g m}^{-3}$  due to adopting cool roofs, which they compute would result in an increase of 2/3  
334 exceedance day for the 24-hr federal  $\text{PM}_{2.5}$  standard. (The number of exceedance days is not an  
335 integer because they report 3x3 cell moving averages.) Thus, even though these changes may look  
336 small, they have the potential to increase the annual number of days exceeding air quality standards  
337 and are therefore important for regulatory agencies in controlling  $\text{PM}_{2.5}$  pollution.

### 338 3.5 Mechanisms that lead to changes in $\text{PM}_{2.5}$ concentrations

339 As mentioned in the introduction, adopting cool surfaces can influence  $\text{PM}_{2.5}$  concentrations  
340 mainly via (1) reducing ventilation, (2) slowing temperature dependent reactions and emissions,  
341 and (3) increasing the likelihood that semi-volatile species will partition to particle phase. In the  
342 following sections we report on the relative importance of these pathways.

#### 343 3.5.1 Ventilation

344 For primary pollutants such as elemental carbon (EC), mass concentrations depend highly on  
345 ventilation and are insensitive to atmospheric chemistry in the model. (Note that strictly speaking,  
346 hydrophilic species can coat EC and increase its hygroscopicity, enabling the in-cloud wet  
347 scavenging of EC<sup>56</sup>. This so-called “aging process” depends on temperature-dependent  
348 atmospheric photochemical reactions that form hydrophilic species, such as sulfate. However, the

349 aging of EC should not be a very important process during summer when there is little precipitation  
350 in the Los Angeles Basin.) Decreases in ventilation (Section 3.1) impede the dilution and transport  
351 of pollutants in source regions and may also reduce dry deposition, leading to increases in near-  
352 surface pollutant concentrations. This ventilation effect is driven by vertical and horizontal mixing  
353 of pollutants in the planetary boundary layer, which can be investigated using PBL height and  
354 surface wind speeds, respectively. Figure 5 shows that fractional increase in EC is positively  
355 correlated with the fractional reductions in PBL height and 10-meter wind speed. Fractional  
356 reduction in PBL height can explain 42% of the variability in the fractional increase in EC  
357 concentrations for both COOL\_WALL – CONTROL and COOL\_ROOF – CONTROL. Fractional  
358 reduction in horizontal wind speed explains 17% (79%) of the variability in fractional increase of  
359 EC concentrations due to adopting cool walls (roofs).

### 360 3.5.2 Quantifying the relative importance of ventilation versus other factors for driving 361 changes in PM

362 Following the method described in Section 2.5, we quantify increases in PM<sub>2.5</sub> species that can be  
363 attributed to reductions in ventilation and changes in other processes. As indicated in Figure 4,  
364 after removing the effects of ventilation, the change in spatially averaged EC and POA is close to  
365 zero. Therefore, increases in primary pollutant (EC and POA) concentrations are attributable to  
366 suppressed ventilation. A large fraction of the increase in sulfate from cool surface adoption can  
367 be attributed to suppressed ventilation. Other driving processes can affect sulfate concentrations:  
368 (a) reductions in temperature-dependent reaction rates would decrease sulfate production; and (b)  
369 changes in cloud cover can also influence in-cloud SO<sub>2</sub> oxidation, which occurs faster than gas-  
370 phase oxidation of SO<sub>2</sub> if clouds are present. When the ventilation effect is excluded, sulfate  
371 concentrations slightly increase from 04:00 to 14:00 LST but decrease at most other hours, due to

372 adopting cool surfaces. Nevertheless, ventilation is the dominant process leading to sulfate  
373 increases, contributing to 76 % (91%) of the daily average increase for COOL\_WALL –  
374 CONTROL (COOL\_ROOF – CONTROL).

375 On the other hand, the ventilation effect accounts for a small portion of the increase in semi-volatile  
376 species such as nitrate and ammonium (in the form of ammonium nitrate). Concentrations of these  
377 particulate species rise drastically even when the ventilation effect is excluded. This is because the  
378 reaction between gas-phase ammonia and nitric acid that forms particulate nitrate is reversible, and  
379 the equilibrium constant for the reaction is highly temperature dependent. Temperature reductions  
380 would cause gas to particle conversion and increase the concentrations of ammonium nitrate<sup>26</sup>.  
381 Note that the amount of nitrate at equilibrium has a non-linear relationship with temperature. Thus,  
382 the relationship between increase in nitrate concentration due to gas-to-particle conversion (Figure  
383 4) and temperature reduction is not linear; the increase in nitrate depends not only on the magnitude  
384 of temperature reduction but also the baseline temperature. In contrast to shifting equilibrium of  
385 the reaction between nitric acid and ammonia, which would increase nitrate, cool surfaces adoption  
386 may also reduce photochemistry and impede the formation of nitric acid precursors (i.e., OH and  
387 NO<sub>2</sub>) during the day, leading to a reduction in nitrate. Increased gas-to-particle conversion and  
388 suppressed ventilation outweigh reductions in photochemistry, leading to overall increases in  
389 nitrate concentrations (Figure 4).

390 For secondary organic aerosols (SOA), reductions in ventilation should lead to increases in SOA,  
391 while temperature decreases would be expected to cause (a) increases in gas-to-particle conversion  
392 for semi-volatile species, which would lead to SOA increases, and (b) reduced rates of  
393 temperature-dependent reactions, which would lead to SOA decreases. Biogenic SOA may also  
394 be influenced by reductions in temperature dependent VOC emissions (e.g., isoprene) from

395 vegetation (Figure S11). As shown in Figure 4, both anthropogenic and biogenic SOA increase  
396 when including the influence of changes in ventilation, but decrease when ventilation changes are  
397 excluded. Daily average SOA concentrations increase by 0.018 (0.046)  $\mu\text{g m}^{-3}$  for COOL\_WALL  
398 (COOL\_ROOF) relative to CONTROL. After removing the ventilation effect, daily average SOA  
399 concentrations decrease by 0.057 (0.071)  $\mu\text{g m}^{-3}$  for COOL\_WALL (COOL\_ROOF) relative to  
400 CONTROL. This means that SOA reductions induced by slowed temperature dependent reactions  
401 and biogenic emissions outweigh the expected increases in semi-volatile SOA species due to phase  
402 partitioning. On the other hand, increases in SOA due to suppressed ventilation and increased gas-  
403 to-particle conversion outweigh decreases in SOA due to reduced reaction and emission rates.  
404 These competing effects lead to an overall increase in SOA concentrations, although fractional  
405 increases are small relative to other species.

406 In this paper, we discuss the climate and air quality implications of cool roofs and cool walls,  
407 which have been used in cities to reduce temperatures and thus combat global warming and urban  
408 heat islands. Our results show that reductions in urban surface temperatures lead to both co-  
409 benefits of reduced ozone concentrations and penalties of increased  $\text{PM}_{2.5}$  concentrations,  
410 potentially changing the exceedance days of federal air quality standard in the Los Angeles Basin.  
411 We suggest further studies to assess the air quality effects of other heat strategies and the effects  
412 in other cities. For policy makers, it is important to assess the effects of environmental solutions  
413 from a systematic perspective, i.e., looking at heat mitigation impacts not just from a climate  
414 perspective but also from an air quality perspective.

415

## 416 Acknowledgements

417 This research was supported by the California Energy Commission under contract EPC-14-010,  
418 and the National Science Foundation under grants CBET-1512429 and 1752522. This work was  
419 also supported by the Assistant Secretary for Energy Efficiency and Renewable Energy, Building  
420 Technologies Office of the U.S. Department of Energy under Contract No. DE-AC02-05CH11231.  
421 Computation for the work described in this paper was supported by the University of Southern  
422 California's Center for High-Performance Computing (<https://hpcc.usc.edu/>). We thank Scott  
423 Epstein and Sang-Mi Lee at South Coast Air Quality Management District for providing us  
424 emission datasets. We also thank Pouya Vahmani, Haley Gilbert, Pablo Rosado, Hugo Destailats,  
425 and Xiaochen Tang at Lawrence Berkeley National Laboratory, Dan Li at Boston University,  
426 Ravan Ahmadov and Stu McKeen at National Oceanic and Atmospheric Administration, Joachim  
427 Fallmann at Johannes Gutenberg University Mainz, Gert-Jan Steeneveld at Wageningen  
428 University, and Jan Kleissl at University of California, San Diego for their helpful suggestions.

## 429 Supporting Information

430 Model evaluation, description of the simulated period, and further detail on results. This material  
431 is available free of charge via the Internet at <http://pubs.acs.org>.

432

## 433 References

434 (1) Seto, K. C.; Guneralp, B.; Hutyra, L. R. Global Forecasts of Urban Expansion to 2030 and Direct

- 435 Impacts on Biodiversity and Carbon Pools. *Proc. Natl. Acad. Sci.* **2012**, *109* (40), 16083–16088.
- 436 (2) Oke, T. R. City Size and the Urban Heat Island. *Atmos. Environ. Pergamon Pres* **1973**, *7*, 769–  
437 779.
- 438 (3) Civerolo, K.; Hogrefe, C.; Lynn, B.; Rosenthal, J.; Ku, J. Y.; Solecki, W.; Cox, J.; Small, C.;  
439 Rosenzweig, C.; Goldberg, R.; Knowlton, K.; Kinney, P. Estimating the Effects of Increased  
440 Urbanization on Surface Meteorology and Ozone Concentrations in the New York City  
441 Metropolitan Region. *Atmos. Environ.* **2007**, *41* (9), 1803–1818.
- 442 (4) Li, J.; Georgescu, M.; Hyde, P.; Mahalov, A.; Moustauoui, M. Achieving Accurate Simulations of  
443 Urban Impacts on Ozone at High Resolution. *Environ. Res. Lett.* **2014**, *9* (11), 114019.
- 444 (5) Wang, X. M.; Lin, W. S.; Yang, L. M.; Deng, R. R.; Lin, H. A Numerical Study of Influences of  
445 Urban Land-Use Change on Ozone Distribution over the Pearl River Delta Region, China. *Tellus*  
446 *B Chem. Phys. Meteorol.* **2007**, *59* (3), 633–641.
- 447 (6) Stone, B. Urban Sprawl and Air Quality in Large US Cities. *J. Environ. Manage.* **2008**, *86* (4),  
448 688–698.
- 449 (7) Zhong, S.; Qian, Y.; Sarangi, C.; Zhao, C.; Leung, R.; Wang, H. Urbanization Effect on Winter  
450 Haze in the Yangtze River Delta Region of China. *Geophys. Res. Lett.* **2018**, *45* (13), 6710–6718.
- 451 (8) Tao, W.; Liu, J.; Ban-Weiss, G. A.; Hauglustaine, D. A.; Zhang, L.; Zhang, Q.; Cheng, Y.; Yu, Y.;  
452 Tao, S. Effects of Urban Land Expansion on the Regional Meteorology and Air Quality of Eastern  
453 China. *Atmos. Chem. Phys.* **2015**, *15* (15), 8597–8614.
- 454 (9) Tao, W.; Liu, J.; Ban-Weiss, G. A.; Zhang, L.; Zhang, J.; Yi, K.; Tao, S. Potential Impacts of  
455 Urban Land Expansion on Asian Airborne Pollutant Outflows. *J. Geophys. Res.* **2017**, *122* (14),  
456 7646–7663.
- 457 (10) Sarrat, C.; Lemonsu, A.; Masson, V.; Guedalia, D. Impact of Urban Heat Island on Regional

- 458 Atmospheric Pollution. *Atmos. Environ.* **2006**, *40* (10), 1743–1758.
- 459 (11) Li, Y.; Zhang, J.; Sailor, D. J.; Ban-weiss, G. A. Effects of Urbanization on Regional Meteorology  
460 and Air Quality in Southern California. *Atmos. Chem. Phys.* **2019**, *19* (7), 4439–4457.
- 461 (12) Rosenfeld, A. H.; Akbari, H.; Romm, J. J.; Pomerantz, M. Cool Communities: Strategies for Heat  
462 Island Mitigation and Smog Reduction. *Energy Build.* **1998**, *28* (1), 51–62.
- 463 (13) Taha, H. Meso-Urban Meteorological and Photochemical Modeling of Heat Island Mitigation.  
464 *Atmos. Environ.* **2008**, *42* (38), 8795–8809.
- 465 (14) Taha, H.; Chang, S.; Akbari, H. Meteorological and Air Quality Impacts of Heat Island Mitigation  
466 Measures in Three U.S. Cities. *Energy* **2000**, No. April.
- 467 (15) Taha, H. Meteorological, Air-Quality, and Emission-Equivalence Impacts of Urban Heat Island  
468 Control in California. *Sustain. Cities Soc.* **2015**, *19*, 207–221.
- 469 (16) Zhang, J.; Zhang, K.; Liu, J.; Ban-Weiss, G. Revisiting the Climate Impacts of Cool Roofs around  
470 the Globe Using an Earth System Model. *Environ. Res. Lett.* **2016**, *11* (8), 084014.
- 471 (17) Mohegh, A.; Rosado, P.; Jin, L.; Millstein, D.; Levinson, R.; Ban-Weiss, G. Modeling the Climate  
472 Impacts of Deploying Solar Reflective Cool Pavements in California Cities. *J. Geophys. Res.*  
473 **2017**, *122* (13), 6798–6817.
- 474 (18) Taha, H.; Konopacki, S.; Gabersek, S. Impacts of Large-Scale Surface Modifications on  
475 Meteorological Conditions and Energy Use: A 10-Region Modeling Study. *Theor. Appl. Climatol.*  
476 **1999**, *62* (3–4), 175–185.
- 477 (19) Georgescu, M.; Morefield, P. E.; Bierwagen, B. G.; Weaver, C. P. Urban Adaptation Can Roll  
478 Back Warming of Emerging Megapolitan Regions. *Proc. Natl. Acad. Sci.* **2014**, *111* (8), 2909–  
479 2914.



- 480 (20) Li, D.; Bou-Zeid, E.; Oppenheimer, M. The Effectiveness of Cool and Green Roofs as Urban Heat  
481 Island Mitigation Strategies. *Environ. Res. Lett.* **2014**, *9* (5), 055002.
- 482 (21) Vahmani, P.; Ban-Weiss, G. Climatic Consequences of Adopting Drought-Tolerant Vegetation  
483 over Los Angeles as a Response to California Drought. *Geophys. Res. Lett.* **2016**, *43* (15), 8240–  
484 8249.
- 485 (22) Mohegh, A.; Levinson, R.; Taha, H.; Gilbert, H.; Zhang, J.; Li, Y.; Tang, T.; Ban-Weiss, G.  
486 Observational Evidence of Neighborhood Scale Reductions in Air Temperature Associated with  
487 Increases in Roof Albedo. *Climate* **2018**, *6* (4), 98.
- 488 (23) Epstein, S. A.; Lee, S.-M.; Katzenstein, A. S.; Carreras-Sospedra, M.; Zhang, X.; Farina, S. C.;  
489 Vahmani, P.; Fine, P. M.; Ban-Weiss, G. Air-Quality Implications of Widespread Adoption of  
490 Cool Roofs on Ozone and Particulate Matter in Southern California. *Proc. Natl. Acad. Sci.* **2017**,  
491 201703560.
- 492 (24) Nowak, D. J.; McHale, P. J.; Ibarra, M.; Crane, D.; Stevens, J. C.; Luley, C. J. Modeling the  
493 Effects of Urban Vegetation on Air Pollution. *Air Pollut. Model. its Appl. XII* **1998**, 399–407.
- 494 (25) Taha, H. Modeling the Impacts of Large-Scale Albedo Changes on Ozone Air Quality in the South  
495 Coast Air Basin. *Atmos. Environ.* **1997**, *31* (11), 1667–1676.
- 496 (26) Moya, M.; Ansari, A. S.; Pandis, S. N. Partitioning of Nitrate and Ammonium between the Gas  
497 and Particulate Phases during the 1997 IMADA-AVER Study in Mexico City. *Atmos. Environ.*  
498 **2001**, *35* (10), 1791–1804.
- 499 (27) Pun, B. K.; Griffin, R. J.; Seigneur, C.; Seinfeld, J. H. Secondary Organic Aerosol 2.  
500 Thermodynamic Model for Gas/Particle Partitioning of Molecular Constituents. *J. Geophys. Res.*  
501 *Atmos.* **2002**, *107* (D17), AAC-4.
- 502 (28) Taha, H. Urban Surface Modification as a Potential Ozone Air-Quality Improvement Strategy in

- 503 California: A Mesoscale Modelling Study. *Boundary-Layer Meteorol.* **2008**, *127* (2), 219–239.
- 504 (29) Zhang, J.; Moheg, A.; Li, Y.; Levinson, R.; Ban-Weiss, G. Systematic Comparison of the  
505 Influence of Cool Wall versus Cool Roof Adoption on Urban Climate in the Los Angeles Basin.  
506 *Environ. Sci. Technol.* **2018**, *52* (19), 11188–11197.
- 507 (30) Grell, G. A.; Peckham, S. E.; Schmitz, R.; McKeen, S. A.; Frost, G.; Skamarock, W. C.; Eder, B.  
508 Fully Coupled “Online” Chemistry within the WRF Model. *Atmos. Environ.* **2005**, *39* (37), 6957–  
509 6975.
- 510 (31) Chen, D.; Li, Q.; Stutz, J.; Mao, Y.; Zhang, L.; Pikelnaya, O.; Tsai, J. Y.; Haman, C.; Lefer, B.;  
511 Rappenglück, B.; Alvarez, S. L.; Neuman, J. A.; Flynn, J.; Roberts, J. M.; Nowak, J. B.; de Gouw,  
512 J.; Holloway, J.; Wagner, N. L.; Veres, P.; Brown, S. S.; Ryerson, T. B.; Warneke, C.; Pollack, I.  
513 B. WRF-Chem Simulation of NO<sub>x</sub> and O<sub>3</sub> in the L.A. Basin during CalNex-2010. *Atmos.*  
514 *Environ.* **2013**, *81*, 421–432.
- 515 (32) Kim, S. W.; Heckel, A.; Frost, G. J.; Richter, A.; Gleason, J.; Burrows, J. P.; McKeen, S.; Hsie, E.  
516 Y.; Granier, C.; Trainer, M. NO<sub>2</sub> Columns in the Western United States Observed from Space and  
517 Simulated by a Regional Chemistry Model and Their Implications for NO<sub>x</sub> Emissions. *J. Geophys.*  
518 *Res. Atmos.* **2009**, *114* (11), 1–29.
- 519 (33) Mlawer, E. J.; Taubman, S. J.; Brown, P. D.; Iacono, M. J.; Clough, S. A. Radiative Transfer for  
520 Inhomogeneous Atmospheres: RRTM, a Validated Correlated-k Model for the Longwave. *J.*  
521 *Geophys. Res. Atmos.* **1997**, *102* (D14), 16663–16682.
- 522 (34) Chou, M.; Suarez, M. J. A Solar Radiation Parameterization for Atmospheric Studies. Technical  
523 Report Series on Global Modeling and Data Assimilation 1999.
- 524 (35) Lin, Y.-L.; Farley, R. D.; Orville, H. D.; Lin, Y.-L.; Farley, R. D.; Orville, H. D. Bulk  
525 Parameterization of the Snow Field in a Cloud Model. *J. Clim. Appl. Meteorol.* **1983**, *22* (6),

- 526 1065–1092.
- 527 (36) Grell, G. A.; Dévényi, D. A Generalized Approach to Parameterizing Convection Combining  
528 Ensemble and Data Assimilation Techniques. *Geophys. Res. Lett.* **2002**, *29* (14), 38-1-38–4.
- 529 (37) Hong, S.-Y.; Noh, Y.; Dudhia, J. A New Vertical Diffusion Package with an Explicit Treatment of  
530 Entrainment Processes. *Mon. Weather Rev.* **2006**, *134* (9), 2318–2341.
- 531 (38) Wickham, J. D.; Stehman, S. V.; Gass, L.; Dewitz, J.; Fry, J. A.; Wade, T. G. Accuracy  
532 Assessment of NLCD 2006 Land Cover and Impervious Surface. *Remote Sens. Environ.* **2013**,  
533 *130*, 294–304.
- 534 (39) Fry, J. A.; Xian, G.; Jin, S.; Dewitz, J. A.; Homer, C. G.; Yang, L.; Barnes, C. A.; Herold, N. D.;  
535 Wickham, J. D. Completion of the 2006 National Land Cover Database for the Conterminous  
536 United States. *Photogramm. Eng. Remote Sensing* **2011**, *77*, 858–566.
- 537 (40) Chen, F.; Dudhia, J.; Chen, F.; Dudhia, J. Coupling an Advanced Land Surface–Hydrology Model  
538 with the Penn State–NCAR MM5 Modeling System. Part I: Model Implementation and  
539 Sensitivity. *Mon. Weather Rev.* **2001**, *129* (4), 569–585.
- 540 (41) Kusaka, H.; Kondo, H.; Kikegawa, Y.; Kimura, F. A Simple Single-Layer Urban Canopy Model  
541 for Atmospheric Models: Comparison with Multi-Layer and Slab Models. *Boundary-Layer*  
542 *Meteorol.* **2001**, *101* (3), 329–358.
- 543 (42) Ching, J.; Brown, M.; Burian, S.; Chen, F.; Cionco, R.; Hanna, A.; Hultgren, T.; McPherson, T.;  
544 Sailor, D.; Taha, H.; Williams, D. National Urban Database and Access Portal Tool. *Bull. Am.*  
545 *Meteorol. Soc.* **2009**, *90* (8), 1157–1168.
- 546 (43) LARIAC. Countywide Building Outlines <https://egis3.lacounty.gov/dataportal/lariac/> (accessed Jul  
547 11, 2017).
- 548 (44) CAMS. LA County Street & Address File <https://egis3.lacounty.gov/dataportal/2014/06/16/2011->

- 549 la-county-street-centerline-street-address-file (accessed Aug 3, 2017).
- 550 (45) Fallmann, J.; Forkel, R.; Emeis, S. Secondary Effects of Urban Heat Island Mitigation Measures  
551 on Air Quality. *Atmos. Environ.* **2016**, *125*, 199–211.
- 552 (46) Stockwell, W. R.; Kirchner, F.; Kuhn, M.; Seefeld, S. A New Mechanism for Regional  
553 Atmospheric Chemistry Modeling. *J. Geophys. Res. Atmos.* **1997**, *102* (D22), 25847–25879.
- 554 (47) Ahmadov, R.; McKeen, S.; Trainer, M.; Banta, R.; Brewer, A.; Brown, S.; Edwards, P. M.; De  
555 Gouw, J. A.; Frost, G. J.; Gilman, J.; Helmig, D.; Johnson, B.; Karion, A.; Koss, A.; Langford, A.;  
556 Lerner, B.; Olson, J.; Oltmans, S.; Peischl, J.; Pétron, G.; Pichugina, Y.; Roberts, J. M.; Ryerson,  
557 T.; Schnell, R.; Senff, C.; Sweeney, C.; Thompson, C.; Veres, P. R.; Warneke, C.; Wild, R.;  
558 Williams, E. J.; Yuan, B.; Zamora, R. Understanding High Wintertime Ozone Pollution Events in  
559 an Oil- and Natural Gas-Producing Region of the Western US. *Atmos. Chem. Phys.* **2015**, *15* (1),  
560 411–429.
- 561 (48) Ackermann, I. J.; Hass, H.; Memmesheimer, M.; Ebel, A.; Binkowski, F. S.; Shankar, U. Modal  
562 Aerosol Dynamics Model for Europe Development and First Applications. *Atmos. Environ.* **1998**,  
563 *32* (17), 2981–2999.
- 564 (49) Ahmadov, R.; McKeen, S. A.; Robinson, A. L.; Bahreini, R.; Middlebrook, A. M.; de Gouw, J. A.;  
565 Meagher, J.; Hsie, E.-Y.; Edgerton, E.; Shaw, S.; Trainer, M. A Volatility Basis Set Model for  
566 Summertime Secondary Organic Aerosols over the Eastern United States in 2006. *J. Geophys.*  
567 *Res. Atmos.* **2012**, *117* (D6), n/a-n/a.
- 568 (50) California Air Resources Board. ARB’s Emission Inventory Activities  
569 <https://www.arb.ca.gov/ei/ei.htm> (accessed Jun 18, 2017).
- 570 (51) USEPA. Profile of the 2011 National Air Emissions Inventory (U.S. EPA 2011 NEI Version 1.0).  
571 **2014**, No. April, 23.

- 572 (52) South Coast Air Quality Management District. Final 2016 Air Quality Management Plan,  
573 Appendix III: Base and Future Year Emission Inventory [http://www.aqmd.gov/docs/default-](http://www.aqmd.gov/docs/default-source/clean-air-plans/air-quality-management-plans/2016-air-quality-management-plan/final-2016-aqmp/appendix-iii.pdf)  
574 [source/clean-air-plans/air-quality-management-plans/2016-air-quality-management-plan/final-](http://www.aqmd.gov/docs/default-source/clean-air-plans/air-quality-management-plans/2016-air-quality-management-plan/final-2016-aqmp/appendix-iii.pdf)  
575 [2016-aqmp/appendix-iii.pdf](http://www.aqmd.gov/docs/default-source/clean-air-plans/air-quality-management-plans/2016-air-quality-management-plan/final-2016-aqmp/appendix-iii.pdf) (accessed Jun 18, 2018).
- 576 (53) Guenther, A.; Karl, T.; Harley, P.; Wiedinmyer, C.; Palmer, P. I.; Geron, C. Estimates of Global  
577 Terrestrial Isoprene Emissions Using MEGAN (Model of Emissions of Gases and Aerosols from  
578 Nature). *Atmos. Chem. Phys.* **2006**, *6* (11), 3181–3210.
- 579 (54) Sleiman, M.; Ban-Weiss, G.; Gilbert, H. E.; François, D.; Berdahl, P.; Kirchstetter, T. W.;  
580 Destailhats, H.; Levinson, R. Soiling of Building Envelope Surfaces and Its Effect on Solar  
581 Reflectance - Part I: Analysis of Roofing Product Databases. *Sol. Energy Mater. Sol. Cells* **2011**,  
582 *95* (12), 3385–3399.
- 583 (55) Berdahl, P.; Akbari, H.; Levinson, R.; Miller, W. A. Weathering of Roofing Materials - An  
584 Overview. *Constr. Build. Mater.* **2008**, *22* (4), 423–433.
- 585 (56) Zhang, Q.; Quan, J.; Tie, X.; Li, X.; Liu, Q.; Gao, Y.; Zhao, D. Effects of Meteorology and  
586 Secondary Particle Formation on Visibility during Heavy Haze Events in Beijing, China. *Sci.*  
587 *Total Environ.* **2015**, *502*, 578–584.
- 588 (57) Zhang, J.; Liu, J.; Tao, S.; Ban-Weiss, G. A. Long-Range Transport of Black Carbon to the Pacific  
589 Ocean and Its Dependence on Aging Timescale. *Atmos. Chem. Phys.* **2015**, *15* (20), 11521–11535.
- 590
- 591

592

593

594 Table 1. Spatially averaged meteorological variables and pollutant concentrations for the CONTROL  
 595 scenario, and the change relative to CONTROL for COOL\_WALL and COOL\_ROOF. Values represent  
 596 spatial averages in Los Angeles County (shown in Figure S3b) for urban grid cells from 00:00 LST on July 3  
 597 to 00:00 LST on July 12.

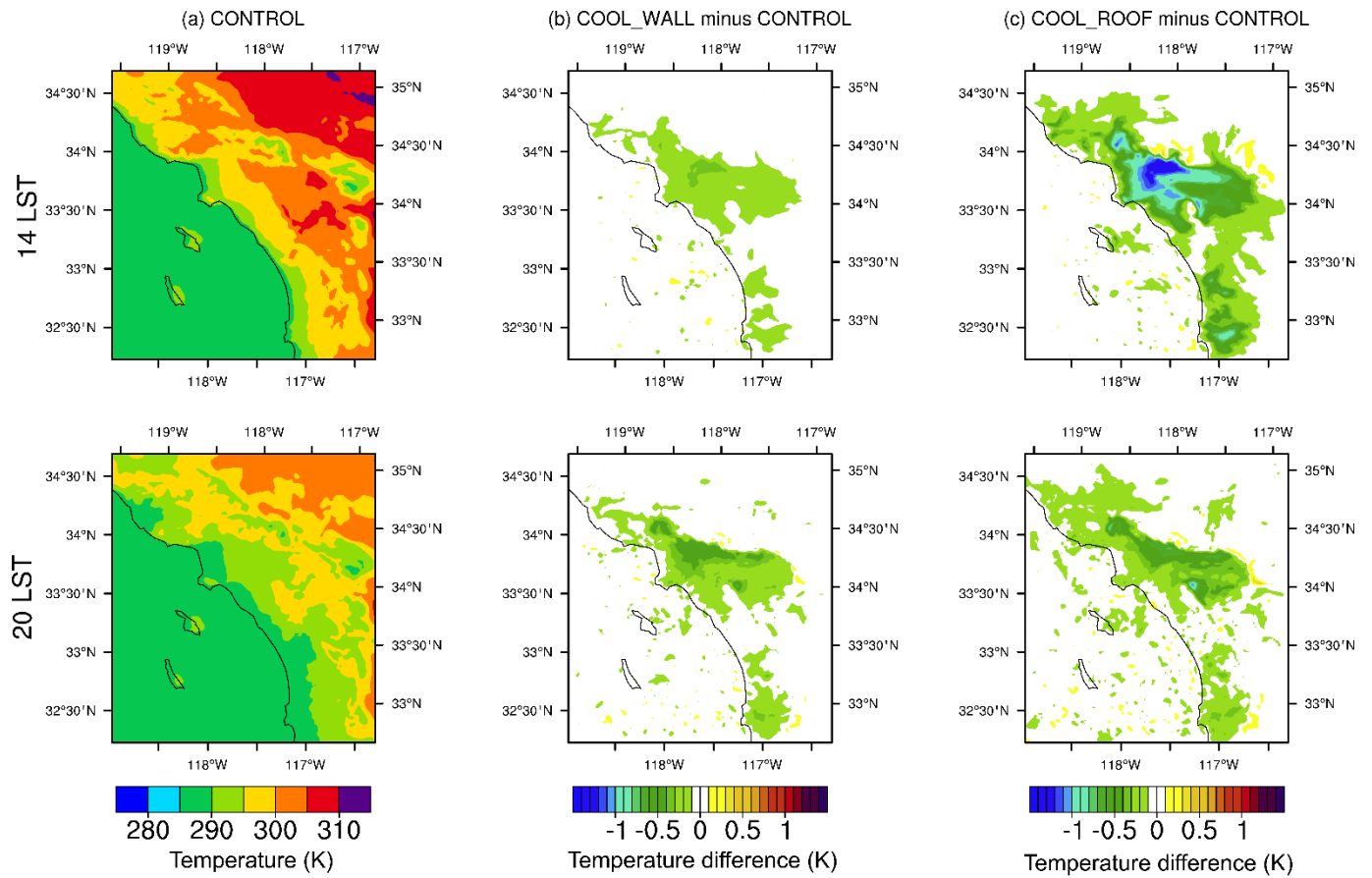
	CONTROL	COOL_WALL minus CONTROL	COOL_ROOF minus CONTROL
Daily average near-surface air temperature <sup>a</sup> (K)	292.85	-0.24	-0.45
10-meter wind speed at 14:00 LST (m s <sup>-1</sup> )	4.15	-0.06	-0.21
10-meter wind speed at 20:00 LST (m s <sup>-1</sup> )	2.28	-0.08	-0.09
Daily maximum 8-hour average ozone concentration (ppbv)	38.47	-0.35	-0.83
Daily average PM <sub>2.5</sub> concentration (μg m <sup>-3</sup> )	12.25	0.62	0.85
Daily average nitrate concentration <sup>b</sup> (μg m <sup>-3</sup> )	0.89	0.11	0.18
Daily average ammonium concentration <sup>b</sup> (μg m <sup>-3</sup> )	0.98	0.07	0.10
Daily average sulfate concentration <sup>b</sup> (μg m <sup>-3</sup> )	1.91	0.11	0.13
Daily average EC concentration <sup>b</sup> (μg m <sup>-3</sup> )	0.87	0.05	0.06
Daily average anthropogenic SOA concentration <sup>b</sup> (μg m <sup>-3</sup> )	1.22	0.01	0.04
Daily average biogenic SOA concentration <sup>b</sup> (μg m <sup>-3</sup> )	0.51	0.01	0.01
Daily average POA concentration <sup>b</sup> (μg m <sup>-3</sup> )	1.90	0.12	0.14

598 <sup>a</sup> Near-surface air temperature refers to the temperature in the lowest atmospheric layer.

599 <sup>b</sup> Mass concentrations for particles with diameter less than 2.5 μm (i.e., nuclei and accumulation mode)  
 600 are included for each species.

601

602



603

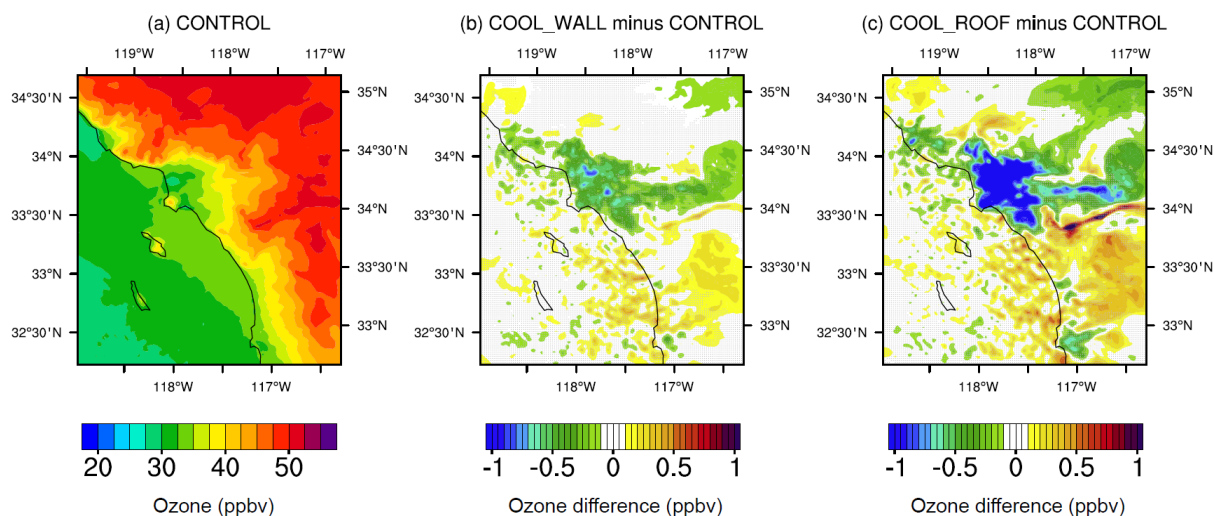
604 Figure 1. Spatially resolved near-surface air temperatures (K) at 14:00 LST and 20:00 LST for (a) the  
605 CONTROL scenario, and the difference relative to CONTROL for (b) COOL\_WALL and (c) COOL\_ROOF.  
606 Values are temporally averaged over the period of 00:00 LST on July 3 to 00:00 LST on July 12.

607

608

609

610

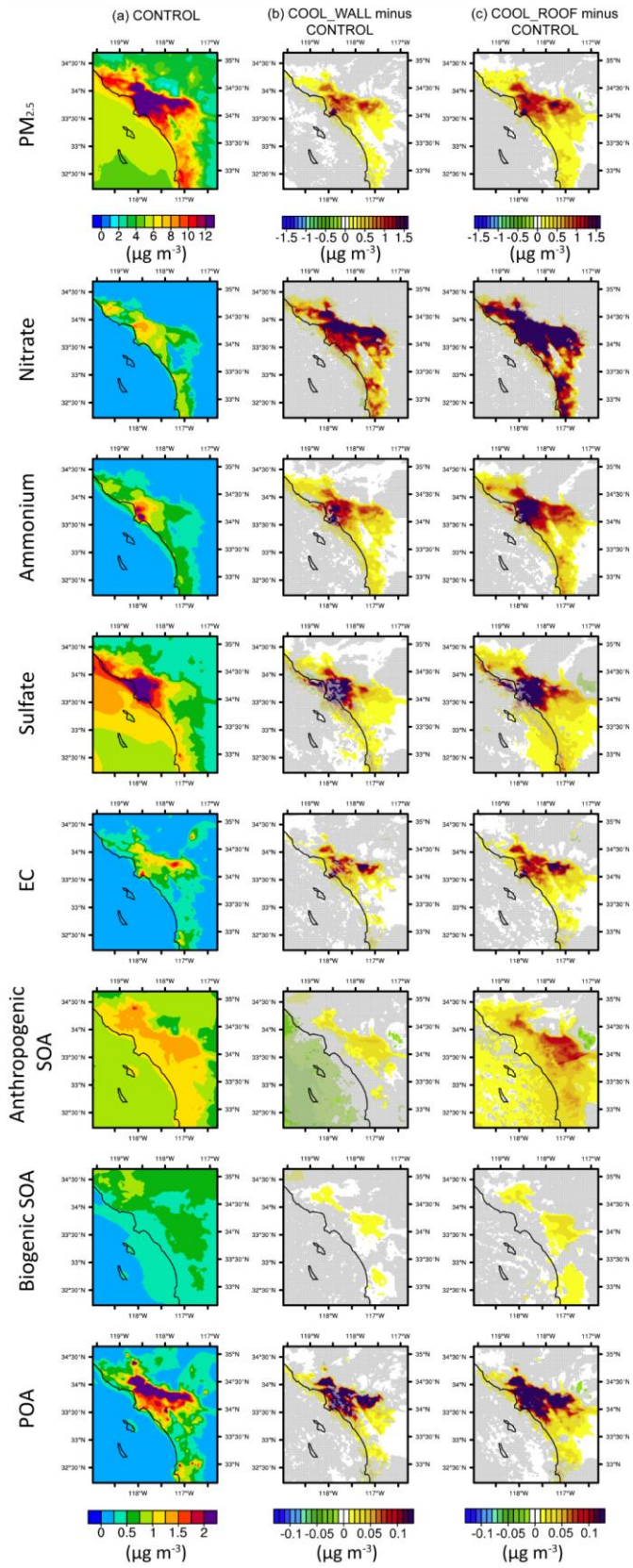


611

612 Figure 2. Spatially resolved daily maximum 8-hour average (MDA8) ozone concentrations (ppbv) for (a)  
613 the CONTROL scenario, and changes relative to CONTROL for (b) COOL\_WALL and (c) COOL\_ROOF.  
614 Changes that are not statistically distinguishable from zero (see section 2.4 for details on statistical  
615 analysis) in (b) and (c) are dotted. Values are temporally averaged over the period of 00:00 LST on July 3  
616 to 00:00 LST on July 12.

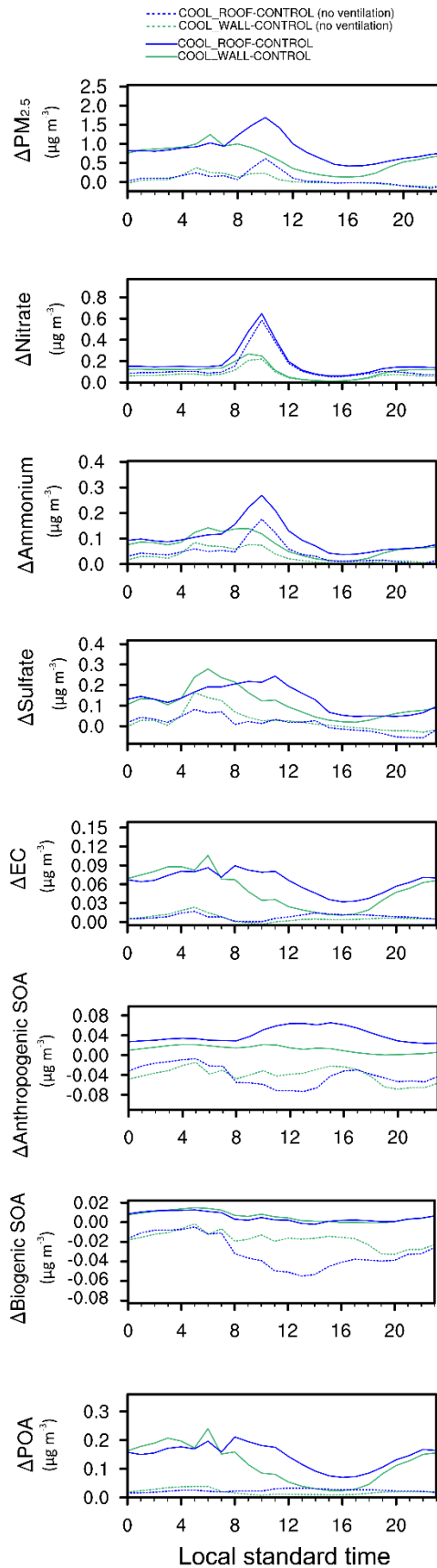
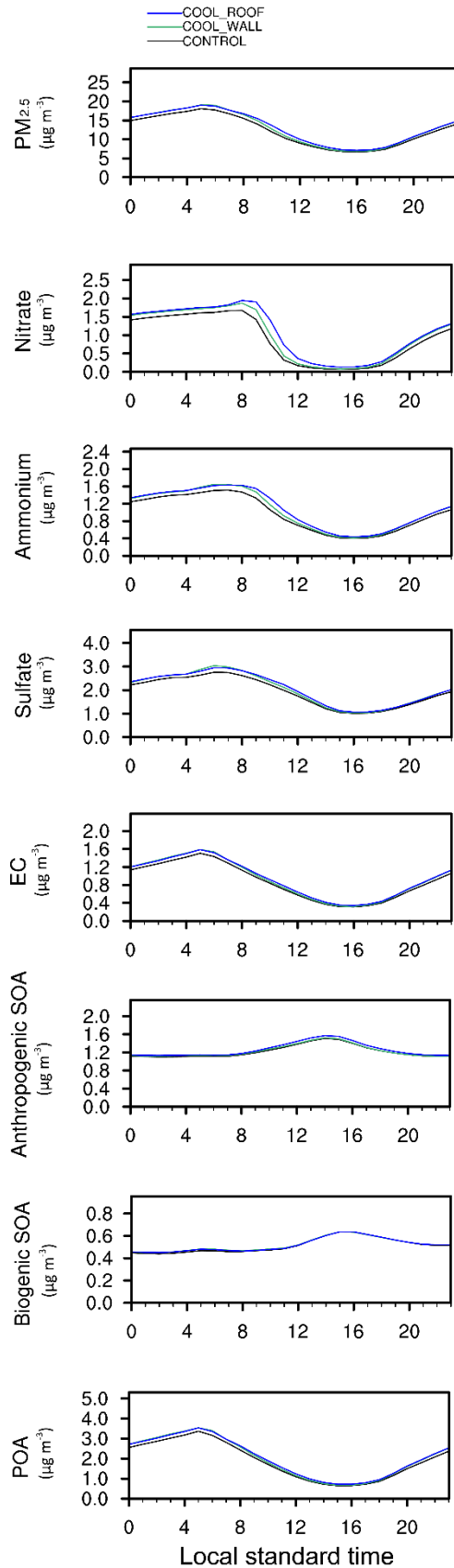
617





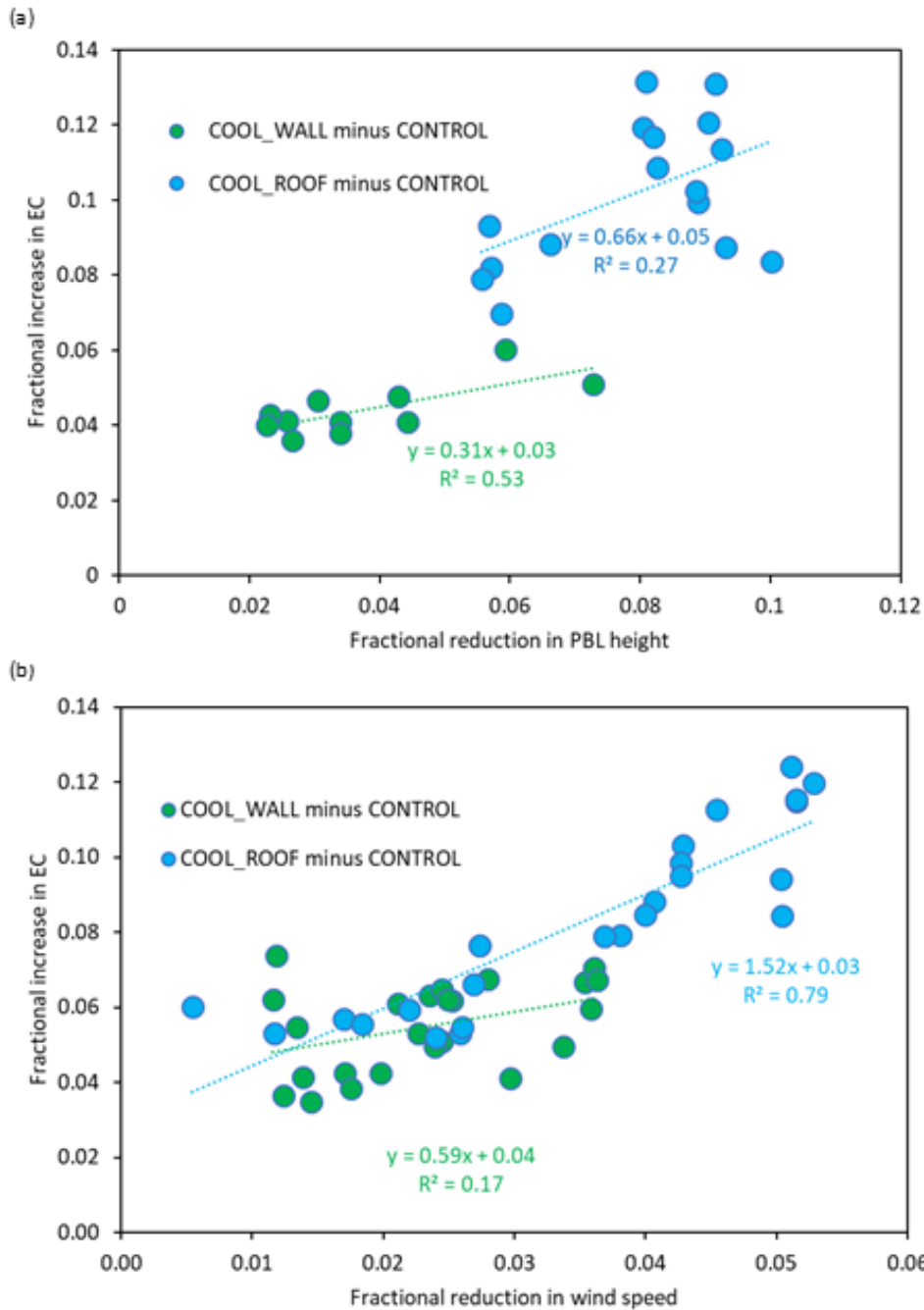
619 Figure 3. Daily average PM<sub>2.5</sub> concentrations ( $\mu\text{g m}^{-3}$ ) by species for CONTROL (left column), as well as  
620 the differences for COOL\_WALL – CONTROL (middle column) and COOL\_ROOF – CONTROL (right  
621 column). Differences that are not statistically distinguishable from zero (see Section 2.4 for details on  
622 statistical analysis) are shaded in gray (middle and right columns of panels). Values are temporally  
623 averaged over the period of 00:00 LST on July 3 to 00:00 LST on July 12.

624



626 Figure 4. Diurnal cycles of spatially averaged PM<sub>2.5</sub> concentrations by species. The left column shows the  
627 diurnal cycle of spatially averaged PM<sub>2.5</sub> ( $\mu\text{g m}^{-3}$ ) for CONTROL, COOL\_WALL, and COOL\_ROOF. The right  
628 column shows the differences in PM<sub>2.5</sub> species for COOL\_WALL – CONTROL and COOL\_ROOF – CONTROL  
629 and the differences if ventilation effect is excluded. Values represent spatial averages in Los Angeles  
630 County (i.e., shown in Figure S3b) for urban grid cells from 00:00 LST on July 3 to 00:00 LST on July 12.  
631 Note that vertical axis ranges vary for each species.

632



633

634 Figure 5. Scatter plots showing fractional increase in EC concentrations induced by cool walls and cool  
 635 roofs versus (a) fractional reduction in PBL height and (b) fractional reduction in 10-meter wind speed.  
 636 The value on each dot represents the hour of day (e.g., 9 = 09:00 LST). Least-squares linear regressions  
 637 and corresponding coefficients of determination ( $R^2$ ) are also shown. Values represent spatial averages  
 638 in Los Angeles County (i.e., shown in Figure S3b) for urban grid cells from 00:00 LST on July 3 to 00:00  
 639 LST on July 12.